Environmental Science & Technology

pubs.acs.org/est

Article

Identifying Quinones in Complex Aqueous Environmental Media (Biochar Extracts) through Tagging with Cysteine and Cysteine-Contained Peptides and High Resolution Mass Spectrometry Analysis

Anil Timilsina, Srinidhi Lokesh, Abrar Shahriar, Travis Numan, Tilman Schramm, Paolo Stincone, Laurinda Korang Nyarko, Christian Dewey, Rene Boiteau, Daniel Petras, and Yu Yang*

Cite This: *Environ. Sci. Technol.* 2024, 58, 16432−16443

Read Online

ACCESS | Metrics & More | Article Recommendations | Supporting Information

ABSTRACT: Quinones are among the most important components in natural organic matter (NOM) for redox reactions; however, no quinones in complex environmental media have been identified. To aid the identification of quinone-containing molecules in ultracomplex environmental samples, we developed a chemical tagging method that makes use of a Michael addition reaction between quinones and thiols (−SH) in cysteine (Cys) and cysteine-contained peptides (CCP). After the tagging, candidates of quinones in representative aqueous environmental samples (water extractions of biochar) were identified through high-resolution mass spectrometry (HRMS) analysis. The MS and UV spectra analysis showed rapid reactions between Cys/CCP and model quinones with β-carbon from the same benzene ring available for Michael addition. The tagging efficiency was not influenced by other co-occurring nonquinone representative compounds, including caffeic acid, cinnamic acid, and coumaric acid. Cys and CCP were used to tag quinones in water extractions of biochars, and possible candidates of quinones (20 and 53 based on tagging with Cys and CCP, respectively) were identified based on the HRMS features for products of reactions with Cys/CCP. This study has successfully demonstrated that such a Michael addition reaction can be used to tag quinones in complex environmental media and potentially determine their identities. The method will enable an in-depth understanding of the redox chemistry of NOM and its critical chemical compositions and structures.

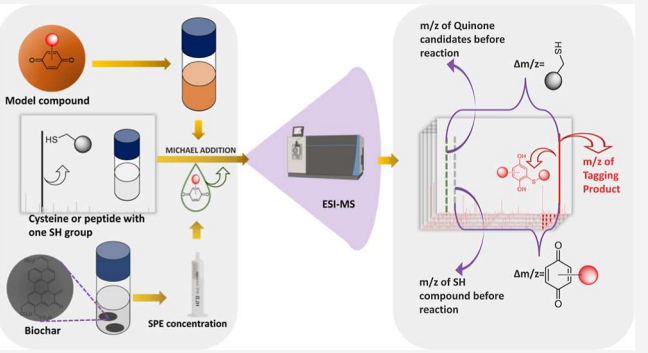

KEYWORDS: *quinone, chemical tagging, Michael addition, cysteine, cysteine-contained peptide, biochar*

INTRODUCTION

Quinones have been argued to be among the most important redox-reactive components of natural organic matter (NOM) in soils and waters.[1−6] NOM can act as an electron donor, acceptor, and shuttle for microbial redox reactions, and quinones are responsible for mediating electron transfer.[2,7−9] The electron shuttling capacity (the ability to electron transfer) of different model quinones, has been linked with their oxidation−reduction potentials.[10] Many quinone biomolecules, including plastoquinone, phylloquinone, riboflavin, nicotinamide adenine dinucleotide, and flavin adenine dinucleotide hydride, that mediate electron transfer in microbial cells have been studied previously, but their presence and relevance in soils remain unclear. In addition to biomolecules, quinones generated during the depolymerization of lignin and other biopolymers are important and could be abundant in NOM. However, the chemical identity of quinone functional groups remains unknown for environmental samples, and thus, their origin is still unclear.

Quinones-mediated redox reactions are important in regulating the biogeochemical cycles of carbon (C),[2,5,11,12] nitrogen (N),[13] and phosphorus (P) by influencing microbial transformation and bioavailability of organic and inorganic compounds.[14,15] Quinones as electron acceptors play a key role in anaerobic microbial methane oxidation[16−19] and therefore can inhibit the release of methane into the atmosphere.[20,21] Reduced quinones (hydroquinones) can be oxidized by iron (Fe) (III) and promote the dissolution of ferric minerals as well as the reductive release of Fe-bound C, N, and P.[8,22−24]

Received: April 23, 2024
Revised: August 26, 2024
Accepted: August 27, 2024
Published: September 3, 2024

In addition to their important roles in the biogeochemical cycles of critical elements, quinones in NOM could promote the redox degradation of contaminants.[25−27] Quinones and their redox reaction products (hydroquinones and semiquinones) have been shown to reduce organohalogens such as CCl_4,[28] bromoform,[29] and hexachloroethane,[30] degrade 2,4,6-trinitrotoluene,[31,32] and activate persulfate for chemical oxidation of polychlorinated benzenes.[33,34] *Geobacter metallireducens*, an important strain capable of degrading organic and inorganic pollutants (vanadium,[35] hexahydro-1,3,5-trinitro-1,3,5-triazine,[36] and chloramphenicol),[37] was shown to grow using anthraquinone disulfonate as the sole terminal electron acceptor.[36,38,39] Biochars have been used for degrading pollutants in water bodies, for which quinones were assigned as critical components for the degradation of toxic chemicals. Lokesh et al. showed that aqueous biochar can be used to degrade triclosan when quinones or semiquinones are the most important reactive components in biochar.[40,41]

The function and behavior of quinone compounds depend on their structures, for instance, when 1,4-benzoquinone (BQ) had a higher reduction potential than anthraquinone-2,5-disulfonate (AQDS), the promotion of hematite reduction was lower by BQ than AQDS.[42] The type of dominant quinones in natural media can vary greatly with strong implications on their environmental functions. Environmental scientists rely on standard quinone compounds, e.g., AQDS, 2-anthraquinone sulfonate, and 2-methyl-1,4-benzoquinone (MBQ), to analyze the roles of quinones in environmental functions,[33,43,44] which can be validated and optimized by determining quinone structures in natural media. Specifically, the redox reactions in natural samples can be reliably predicted or manipulated if the key quinones for electron transfer can be identified.

Till date, despite the importance of quinones in the biogeochemical cycles of critical elements (C, N, P) and transformation of inorganic and organic pollutants as well as engineering applications including the use of biochars, few quinone-containing compounds have been identified in NOM. Quinone identification has been achieved using electron paramagnetic resonance (EPR) spectroscopy analysis, which can distinguish carbon- and oxygen-centered radicals in environmental samples, but cannot reveal the chemical formula or structure.[45] Nuclear magnetic resonance (NMR) spectra, on the other hand, were also used for analyzing model quinones.[46] While NMR is very efficient for de novo structure elucidation, it is challenging to detect quinones at low concentrations in complex environmental samples using NMR.

Recent developments in high-resolution mass spectrometry (HRMS) and tandem mass spectrometry (MS/MS) can shed light on quinones in complex environmental samples.[47,48] HRMS has been used to determine the accurate molecular formula for NOM, but among the extremely diverse components (normally with >2000 HRMS features), it is challenging to identify quinones if they cannot be differentiated from other compounds.[49−51] In addition, many known quinones cannot be efficiently ionized via electron spray ionization (ESI), which is widely used for HRMS analysis. A chemical tag specific to quinones, ionizable by ESI-MS and identifiable by HRMS, would be of great value for such method development. During the ESI ionization, molecules undergo a protonation/deprotonation reaction, which is favored by the presence of electronegative elements, such as O and N, in acidic and basic functional groups as carboxylic acids and amines in Cys and cysteine-contained peptides (CCP). Previous studies have demonstrated that the Michael addition reaction between quinones and cysteine (Cys) can efficiently tag quinones in complex environmental samples for HRMS analysis.[52,53] Ma et al. developed a tagging method with p-benzoquinone (BQ) and methyl-*p*-benzoquinone (MBQ) to identify the Cys-containing proteins.[52] However, the applicability of Cys and CCPs to tag quinones for their structural identification has not been demonstrated for complex aqueous media. Therefore, this study aimed to (1) study the tagging selectivity toward quinone functional groups; (2) study the tagging efficiency in the complex matrix; and (3) identify the chemical formula for possible quinone candidates using HRMS analysis coupled with tagging by Michale addition with Cys and CCP. In brief, this study provides an excellent way of tackling complexity to identify quinones in environmental samples for understanding their redox chemistry and modulating the chemical transformations.

MATERIALS AND METHOD

Chemicals and Materials. High-performance liquid chromatography (HPLC)-grade methanol and acetonitrile were bought from Fisher Scientific (Ward Hill, MA, USA). Model quinones: 1,4-benzoquinone (BQ) was obtained from Alfa Aesar (Shore Road, Heysham, England), 1,4-napthoquinone (NQ), 2-methyl-14-benzoquinone (MBQ), 2-chloro-1,4-benzoquinone (CBQ), and 9,10-anthraquinone-2-carboxylic acid (AQA) were obtained from Sigma-Aldrich (St Louis, MO, USA), and 1,4-anthraquinone (AQ) was obtained from Fisher Scientific (Ward Hill, MA, USA). Additional model compounds for co-occurring chemicals, including coumaric acid (CoA) (with a carboxylic group and phenolic group) and caffeic acid (CaA) (with a carboxylic group and catechol group), were obtained from TCI (Kita-Ku, Tokyo, Japan); and cinnamic acid (CnA) (with a carboxylic group) was obtained from Fisher Scientific (Ward Hill, MA, USA). All these model compounds are with purity > 97%. Cysteine-containing peptide (CCP) ($C_{50}H_{75}N_{15}O_{22}S$, MW = 1269.5) with 11 amino acids (in the sequence of SSDQFRPDDCT) was purchased from BIOMATIK, Kitchener, ON, Canada. Swiss biochar (SB, 500−2000 μm size, pyrolyzed at 700 °C) was obtained from SB (Sarl, Switzerland).

To help clarify the major experimental work and analysis, an overview of tagging reaction and associated analyses is summarized in the Supporting Information, Table S1.

Tagging of Model Quinones. The Michael addition reaction of model quinones with the thiol group in Cys and CCP was examined by mixing them with Cys or CCP in Milli-Q water (≥18.2 MΩ·cm) (Figure S1). BQ (10 mM) stock solution was prepared in Milli-Q water (≥18.2 MΩ·cm), and MBQ (10 mM), CBQ (10 mM), NQ (1 mM), and AQ (1 mM) stock solutions were prepared in acetonitrile/Milli-Q water (50:50%). Reactions (50 μM model compound mixed with 50 μM Cys or CCP) were held at room temperature in a 3 mL quartz cuvette for UV scan, and UV spectra were collected to identify the potential products from the reaction. UV spectra were collected using a UV−vis spectrophotometer (HACH, DR 6000) using 3 mL quartz cuvettes at various time intervals 5, 10, 20, and 30 min (Figure S2); the decay of the original peak and formation of a new peak stopped within 10−15 min. Triplicate scans (190−600 nm) were conducted for each sample. Time-of-flight mass spectrometry (TOF-MS) was used to validate the Michael addition product formed during the reaction.

https://doi.org/10.1021/acs.est.4c04049
Environ. Sci. Technol. 2024, 58, 16432−16443

Reaction Selectivity and Tagging of Quinones in the Presence of Co-occurring Compounds. Other model compounds containing carboxylic/phenolic/catechol functional groups, i.e., CaA, CoA, and CnA, were chosen as model compounds to investigate the thiol group's reactivity and selectivity toward quinone and other naturally co-occurring compounds. These model compounds were mixed individually and all together with Cys to achieve a final concentration of 50 μM for model compounds and 50 μM for Cys. UV spectra were collected and compared between the sample of model compounds and the mixture of model compounds with Cys to verify whether any reaction occurred between these compounds and Cys.

To test if Cys can still be used to tag quinones in the presence of other naturally co-occurring compounds, different concentrations of BQ (10, 50, and 100 μM) were spiked to a mixture of 100 μM CnA, 100 μM CoA, and 100 μM CaA and then reacted with 100 μM Cys in a 1:1 volume ratio. UV and TOF-MS spectra were collected for the mixture after 30 min of reaction.

Chemical Tagging of Quinones Spiked in Biochar Extracts. To validate the efficiency of chemical tagging for quinones in complex environmental samples, Cys and CCP were reacted with BQ spiked in biochar extractions (pH 7.0 ± 0.2). SB was extracted by mixing SB with Mili-Q water (1 g/500 mL) and shaking horizontally at 120 rpm for 1 week. After the shaking, the SB extract (SBE) was obtained by filtering the SB suspension with 0.45 μm glass-fiber filters and stored at 4 °C before use. Dissolved organic carbon (DOC) of the SBE was measured by a Shimadzu TOC/N analyzer (version 1.09.00 © 2011, TOC-L Analyzer), with a value of 144 μM C. BQ (20 μM) was spiked in SBE and reacted with Cys or CCP (20 μM), and the products of the reaction after 30 min were evaluated by TOF-MS analysis.

Analysis of Indigenous Quinones in Biochar Extracts. The solid phase extraction (SPE) concentration/purification process was used to preconcentrate quinones and remove the nonvolatile salts that could lead to diversity in ion adducts or suppress ionization in MS analysis. To enable reliable analysis of SB extract reacted with Cys or CCP, SBE (5 L) was cleaned up and concentrated through SPE using Oasis hydrophilic-lipophilic balanced cartridge (HLB, 6 mL, 500 mg column bead, 60 μm pore size). The SPE cartridge was acidified to pH 3 using concentrated HCL, washed with 10 mL of 100% methanol, and then conditioned with 10 mL of pH 3 Mili-Q water at 15 mL/min. 1−5 mg DOC (<1% of sorbent weight) was loaded onto each cartridge to avoid overloading. Pretreatment of extract might lead to protonation reactions, but minimal or no changes in quinone functional groups were expected. After conditioning, 500 mL of acidified samples was loaded at a 1 mL/min flow rate and eluted with 20 mL acetonitrile/methanol (90:10%). The eluted extracts were evaporated at 40 °C under ultrahigh purity N_2 gas flow at 10 psi and redissolved in 3 mL of 100% methanol. In this way, a large volume of SB extract (5 L) was concentrated to 30 mL (100% methanol), which was further evaporated at 40 °C under ultrahigh purity N_2 gas flow at 10 psi and redissolved in 2.5 mL Mili-Q water. The final 2.5 mL of concentrate of swiss biochar extract (CSBE) was filtered with 0.22 μm sterilized polyvinylidene fluoride filters. The filtered concentrate (45 μL) was diluted to 100 μL and reacted with Cys/CCP (100 μM). The reaction products were evaluated by ultrahigh performance liquid chromatography (Vanquish Horizon) with a high field Orbitrap Mass Spectrometer (Q-Exactive HF) (UHPLC-MS/MS).

TOF-MS Analysis. The reaction samples were analyzed with direct injection electrospray ionization time-of-flight mass spectrometry (20k resolution; Agilent Technologies 6230 TOF LC/MS). The mobile phase including acetonitrile and Mili-Q water (80 and 20%) with 0.1% formic acid, was used at a flow rate of 0.5 mL/min with an injection volume of 20 μL. Positive-mode ESI analyses were conducted at a fragmentation voltage of 150 V with a mass scan range of 50−3000 m/z and a scan rate of 1 spectra/s. The drying gas was set to 325 °C at a flow rate of 5 L/min. The nebulizer pressure was set at 20 psi, and the capillary voltage was maintained at 3500 V. Data acquisition and processing were conducted with a mass accuracy of ±10 ppm and isotope pattern deviation of less than 5%. MestReNova (14.2.0; Santiago de Compostela, Spain) was used to process the TOF-MS data.

LC-Orbitrap MS Analysis and Data Process. LC-Orbitrap MS analyses were performed using a Q-Exactive HF quadrupole orbitrap (Thermo Fisher Scientific, Bremen, Germany) coupled with LC and ESI ionization. The chromatographic separation of 10 μL injected samples was achieved by a C18 core−shell microflow column (Kinetex C18, 150 × 2.1 mm, 1.7 m particle size, 100 A pore size, Phenomenex, Torrance, USA) with a gradient flow of mobile phase A (LC-MS grade H_2O with 0.1% formic acid) and solvent B (LC-MS grade Acetonitrile with 0.1% formic acid) (Supporting Information, Table S2) at 0.5 mL/min flow for 16 min. The orbitrap MS (120k resolution) was operated in positive ESI modes, collecting MS^1 data from m/z 150 to 1500 and MS^2 data of ions with data-dependent acquisition (DDA) mode. The DDA settings were configured as suggested by Stincone et al. (2023).[54] Briefly, the top 5 MS^1 ions were selected for MS^2 fragmentation, dynamic exclusion was enabled, the AGC target was set at 1×10^5, the mass resolving power was set to 30 K, and one microscan was considered for the written scan. The heated electrospray ionization parameters were set as follows: 3.5 KV spray voltage, 250 °C capillary temperature, 50 Arb unit sheath gas flow rate, 12 Arb unit auxiliary gas flow rate, and 400 °C probe temperature.

The data obtained from orbitrap MS were analyzed using MZmine 3.[55] Automated data analysis pipeline (ADAP) chromatograms were developed on MS1 features with 4 minimum consecutive scans and minimum absolute height of 10^4 and 5 ppm m/z error.[56] These ADAP chromatograms were resolved with MS/MS scan pairing, 80% chromatographic threshold, 10^4 minimum absolute height, 1.7 peak ratio of top/edge, 0 to 1 min of peak duration range, and 4 minimum scans. Then features were deisotoped for ^{13}C using 5 ppm m/z tolerance and 0.1 min retention time tolerance. The features table was exported and processed further to identify unique m/z values formed after the reaction and to identify pairs of potential m/z values for apo compounds (quinone suspect before the reaction) and Michael addition product (quinone-Cys/CCP product suspect after the reaction) that have m/z difference of Cys/CCP. The SIRIUS (.mgf) file generated by MZmine 3 was exported for in-silico annotation of molecular formulas[57] and putative structures.

An in-house Python (3.10.2) script was developed and run with a Spyder (v5.4.2)-integrated development environment to screen the features in samples for quinones. As the first step, the features only appearing in the tagged samples were fetched as presumably forming Michael addition product of quinone

https://doi.org/10.1021/acs.est.4c04049
Environ. Sci. Technol. 2024, 58, 16432−16443

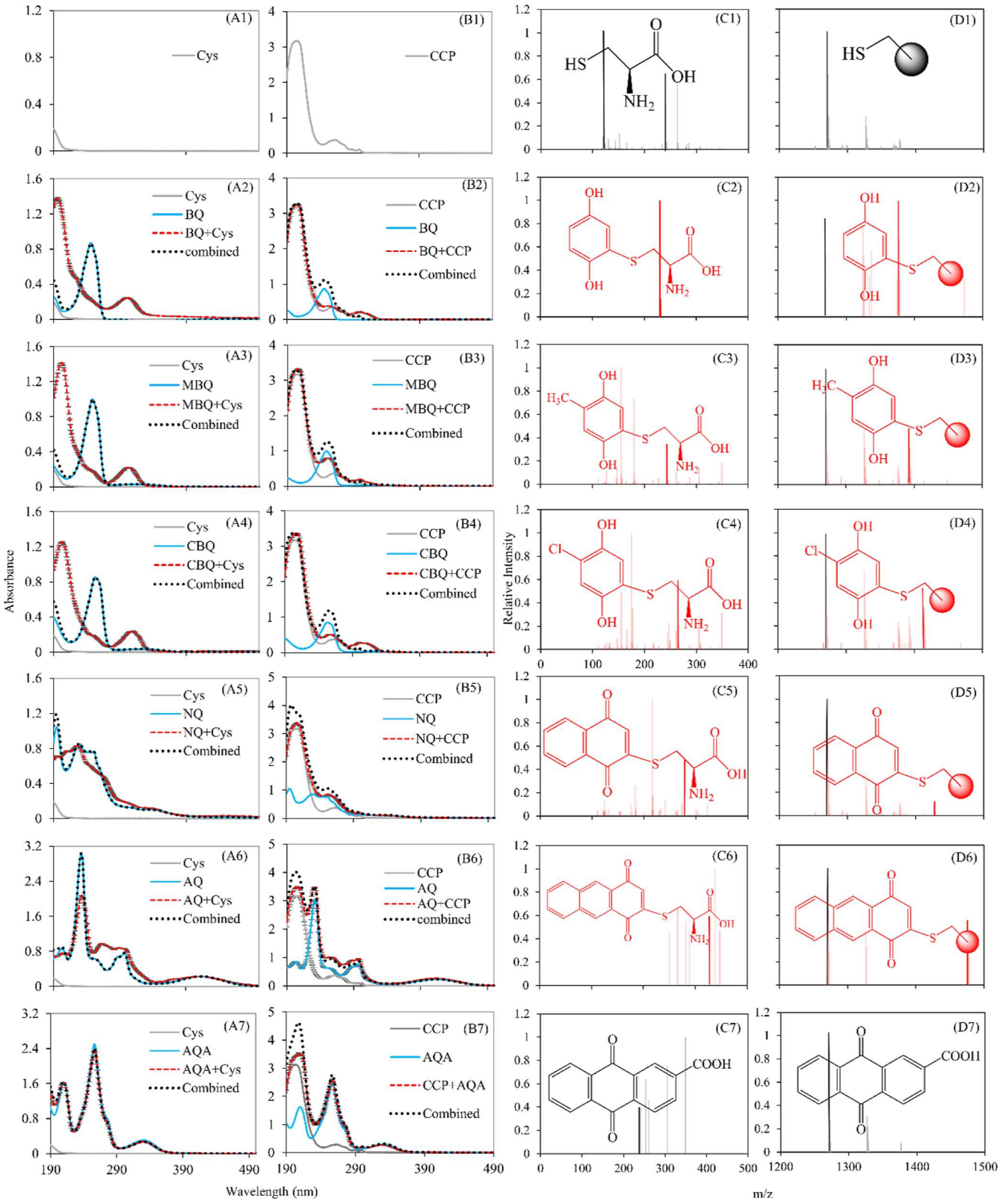

Figure 1. UV-spectra and TOF-MS analysis of Cys and CCP (SSDQFRPDDCT) reacted with model quinones. (A1−A7) UV spectra of Cys and model quinone reaction samples and (C1−C7) MS spectra of Cys (highlighted black) and Cys-quinone reaction products (highlighted red) detected from TOF-MS analysis. (B1−B7) UV spectra of CCP and model quinone reaction samples and (D1−D7) MS spectra of CCP (highlighted black) and CCP-quinone reaction products (highlighted red) detected from TOF-MS analysis. Note: *Y*-error bars in UV spectra show standard deviation of three replicates that may or may not be visible.

and Cys/CCP. The background noise was set as 10^4 for MS^1, and a signal/noise ratio of 3 was used. For peptides, the features were screened for spectra with parent ions $[M + H^+]$ and $[M + 2H^{2+}]$.

https://doi.org/10.1021/acs.est.4c04049
Environ. Sci. Technol. 2024, 58, 16432−16443

Apo-quinones were searched (analysis workflow shown in Figure S3) based on matching the $\Delta m/z$ (eq 1) with the expected values of 121.0198 for tagging with Cys and 1269.4932 for tagging with CCP if hydroquinone (HQ-form) products were formed; 119.0041 for tagging with Cys; and 1267.4775 for tagging with CCP, if quinone (Q-form) products were formed.

$$\Delta m/z = (m/z)_{add} - (m/z)_o \quad (1)$$

where $\Delta m/z$ is the difference in the m/z of features after tagging versus those in original samples; $(m/z)_{add}$ is the m/z of unique features; and $(m/z)_o$ is the m/z of features in the original samples. For the peptide, the value for parent ions of $[M + H^+]$ was used for $(m/z)_{add}$. For the apo-quinones captured with MS^2, the molecular formula was cross-checked with SIRIUS prediction.

Molecular formulas for compounds present in original biochar were assigned using a Python script developed in Visual Code Studio (v1.83). The CoreMS image was created in docker (v4.23.0) and used to run the Python script with the desired modification for mass spectrum parameters. Desired mass spectrum parameters were selected: ion charge range 1−2, mass error in ppm −5 to +5, double bond equivalence (DBE) range 0−40, the elemental composition of $C_{(2-30)}$, $H_{(0-75)}$, $O_{(0-15)}$, and $N_{(0-5)}$, and m/z range for feature picking 100−1000. A Python script was developed to find the matches between apo quinones identified using the $\Delta m/z$ screening code.

RESULTS AND DISCUSSION

Tagging Reaction and Influences of Quinone Structures. UV spectra indicate the rapid reactions between model quinones and Cys or CCP. For BQ, MBQ, and CBQ, the characteristic absorption peaks were observed at 245, 250, and 255 nm, respectively (Figure 1). After 30 min of the reaction with Cys or CCP, the original peaks of quinones were significantly reduced to minimal, when new peaks emerged at 301 nm for the samples of BQ, MBQ, and CBQ, respectively, consistent with the literature report.[58] The new peaks at 301 nm were less significant for the reaction products with CCP. For NQ, there was originally a major peak at 229 nm and a shoulder at 252 nm, when after reacting with Cys, the feature at 252 nm disappeared and a new shoulder peak emerged at 268 nm. When NQ reacted with CCP, the new shoulder peak was overridden by the peak of CCP. For AQ, the original major peak was at 231 nm, when a new peak at 234 nm emerged after the reaction with Cys, and the new peak was less significant for reaction products with peptide, compared to the Beer−Lambert law-based linear combination results of UV spectra (Figure 1). For AQA, the spectra of Cys mixed with AQA were almost exactly the same as those of the linear combination of both, indicating no reactions occurring between Cys and AQA, because of the quinone functional group in AQA fused with side benzene rings and no β carbon available for Michael addition.

The Cys and CCP tagged with quinones were captured by TOF ESI-MS, when most of the original nonsubstituted quinones were poorly ionized under the same condition, except AQA (Figure 1 and Table S3). Cys and Cys−Cys dimer peaks were captured with m/z = 122.0270 and 241.0311 in the standard solution of Cys and the sample of Cys mixed with AQA. New peaks for BQ-Cys, MBQ-Cys, CBQ-Cys, NQ-Cys, and AQ-Cys were captured with m/z of 230.0486, 244.0642, 264.0094, 278.0479, and 328.0634, respectively, corresponding to hydroquinone-Cys for BQ and quinone-Cys for other quinones with more aromatic rings, consistent with previous reports.[59] The highest intensity of the adduct peak was detected for BQ-Cys ($7.4 \times 10^6 \pm 2.3 \times 10^6$), followed by CBQ-Cys, MBQ-Cys, NQ-Cys, and AQ-Cys when the increased molecular size and additional functional groups reduced the intensity by possibly inhibiting the reaction.

Although the formation of new UV peaks for CCP-quinone product formation was less evident compared to those for Cys-quinone products, MS peaks for CCP-quinone products captured were comparable to those of Cys-quinone products. AQA did not react with either tag, confirming that quinones can only be tagged if the β carbon of the core aromatic ring is available for Michael addition. Singly and doubly charged peaks, for BQ-CCP, MBQ-CCP, CBQ-CCP, NQ-CCP, and AQ-CCP products, were captured with higher intensities for doubly charged peaks than singly charged (Supporting Information, Table S3). The MS^1 isotopic pattern was quantitatively compared with the simulated intensity of those isotopes and the formation of those doubly charged ions was validated (Figures S4 and S5). For instance, the peaks were captured for BQ-CCP with m/z of 1378.5247 (intensity of 3.5×10^5) and 689.7690 (intensity of 1.0×10^6), corresponding to the singly and doubly charged products ($[C_{56}H_{79}O_{24}N_{15}S + H]^+$ and $[C_{56}H_{79}O_{24}N_{15}S + 2H]^{2+}$). For $[C_{56}H_{79}O_{24}N_{15}S + 2H]^{2+}$, the major isotope peaks captured were 689.7690, 680.2689, and 680.7672, corresponding to $[^{13}C^{12}C_{55}N_{15}O_{24}S + 2H]^{2+}$, $[^{13}C_2{}^{12}C_{54}N_{15}O_{24}S + 2H]^{2+}$, and $[^{13}C_3{}^{12}C_{53}N_{15}O_{24}S + 2H]^{2+}$. The primary peaks captured for quinone-CCP products were doubly charged ions with an intensity almost double that of singly charged peaks when the peak intensity for singly charged ions of quinone-CCP products was lower than that for quinone-Cys products. Similarly, as quinone-Cys products, the doubly charged ion of BQ-CCP products had the highest intensity of $3.5 \times 10^5 \pm 6.9 \times 10^4$, while AQ-CCP had the lowest intensity of $1.3 \times 10^5 \pm 2.5 \times 10^4$; which is consistent with observations by previous studies where the ionization efficiency was negatively correlated with the molecular size for ESI ionizations. Furthermore, the detection of molecules in various ionized forms, such as $[M + H^+]$ and $[M + 2H^{2+}]$ with (+) ESI, affected the quantitative detection in mass spectrometry, as reported by literature.[60]

The elemental composition and structure of the molecule influence the rate of reaction and the amount of final conversion, which can be explained by the polarity or electron density theory (electrophilicity)[61,62] and stearic hindrance.[63] The type of additional fragment and structure difference can affect the polarity at β-carbon,[64] which influences the Michael addition rate. Furthermore, the detection of molecules in various ionized forms, such as $[M + H^+]$ and $[M + 2H^{2+}]$ with (+) ESI, affected the quantitative detection in mass spectrometry, as reported by literature.[60,65,66] Quinones-Cys products had a major ion peak as $[M + H^+]$ and quinones-CCP had a major ion peak as $[M + 2H^{2+}]$. The AQA and CCP reaction samples did not create a Michael addition peak when tested with HRMS, demonstrating that quinone structures are only able to form quinone peptide when β carbon from the same benzene ring is available for Michael addition. The detectable structures (dominant structure) of tagged quinone can be affected by original quinone structures, where the presence of reduced and oxidized forms of quinones could play a substantial role through their self-reversible redox cycle or

https://doi.org/10.1021/acs.est.4c04049
Environ. Sci. Technol. 2024, 58, 16432−16443

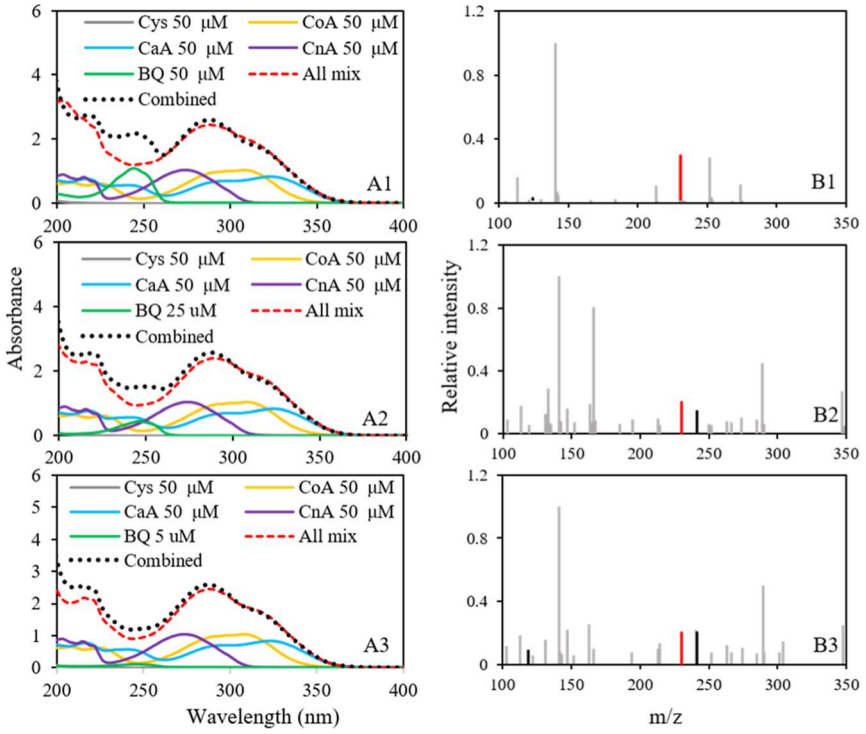

Figure 2. (A1−A3) UV spectra of 50 μM CnA, CaA, and CoA mix spiked with different concentration levels (50, 25, and 5 μM) of 1,4-benzoquinone (BQ) and reacted with Cys, and (B1−B3) MS spectra of 50 μM CnA, CaA, and CoA mix spiked with different concentration levels (50, 25, and 5 μM) of BQ and reacted with Cys. "*All mix*" represents the absorbance of reaction mixture, and "*Combined*" is the sum of absorbance of individual components.

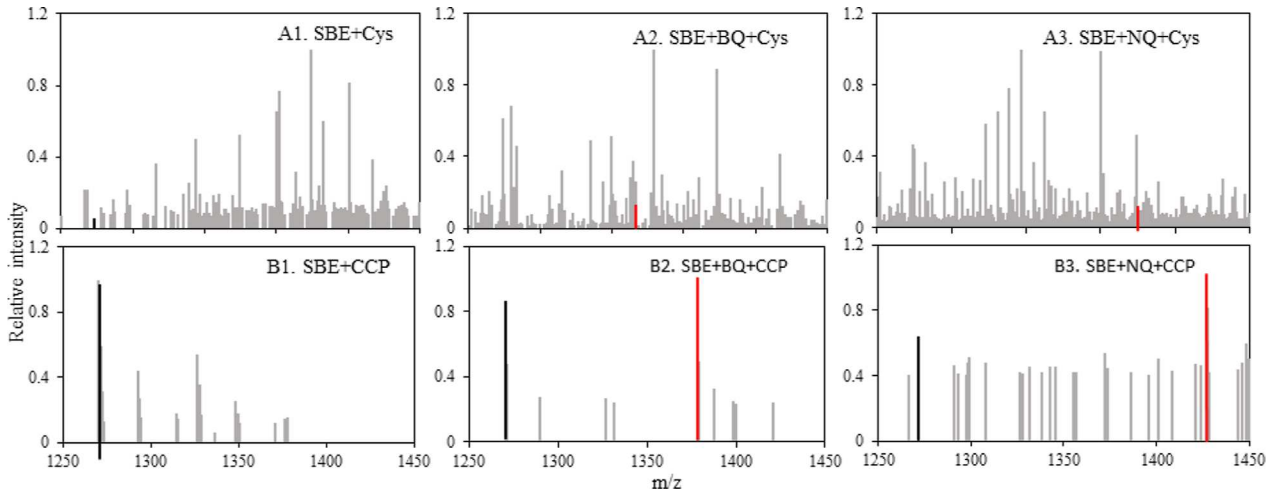

Figure 3. TOF-MS analysis of (A1) SB extract (SBE) and 10 μM Cys reaction, (A2) SBE, 10 μM 1,4-benzoquinone (BQ), and 10 μM Cys reaction, (A3) SBE, 10 μM 1,4-naphthoquinone (NQ), and 10 μM Cys reaction, (B1) SBE and 10 μM CCP reaction, (B2) SBE, 10 μM BQ, and 10 μM CCP reaction, and (B3) SBE, 10 μM NQ, and 10 μM CCP reaction.

cross-reaction with other quinone structures in the pool. In complex samples, quinone moieties are found to be under equilibrium conditions, and considering several factors such as dissolved oxygen, pH, and redox potential of other quinolones and compounds, the dominating structure can be in the hydroquinone or quinone form.[24,67] The presence of oxygen, higher pH, and lower redox potential of quinones favor the stability of oxidized form and vice versa.[68−70] The hydroquinone was found to be stable at neutral conditions, and oxidation required quinone and trace metal ions to catalyze; hence, the autoxidation was kinetically or spin-restricted in the presence of oxygen.[24,71] The additional benzene rings will lower the pK_a due to the resonance effect and could result in more stable quinone in a multicomponent system, and this could be controlled by regulating pH. These quinones could also be prone to the next attack by Cys or CCP when another β carbon is available for Michael addition. As discussed, additional benzene rings to benzoquinones resulted in quinone-Cys and quinone-CCP products predominated by the quinone form, and benzoquinones with no additional benzene ring resulted in products dominated by the hydroquinone form.

https://doi.org/10.1021/acs.est.4c04049
Environ. Sci. Technol. 2024, 58, 16432−16443

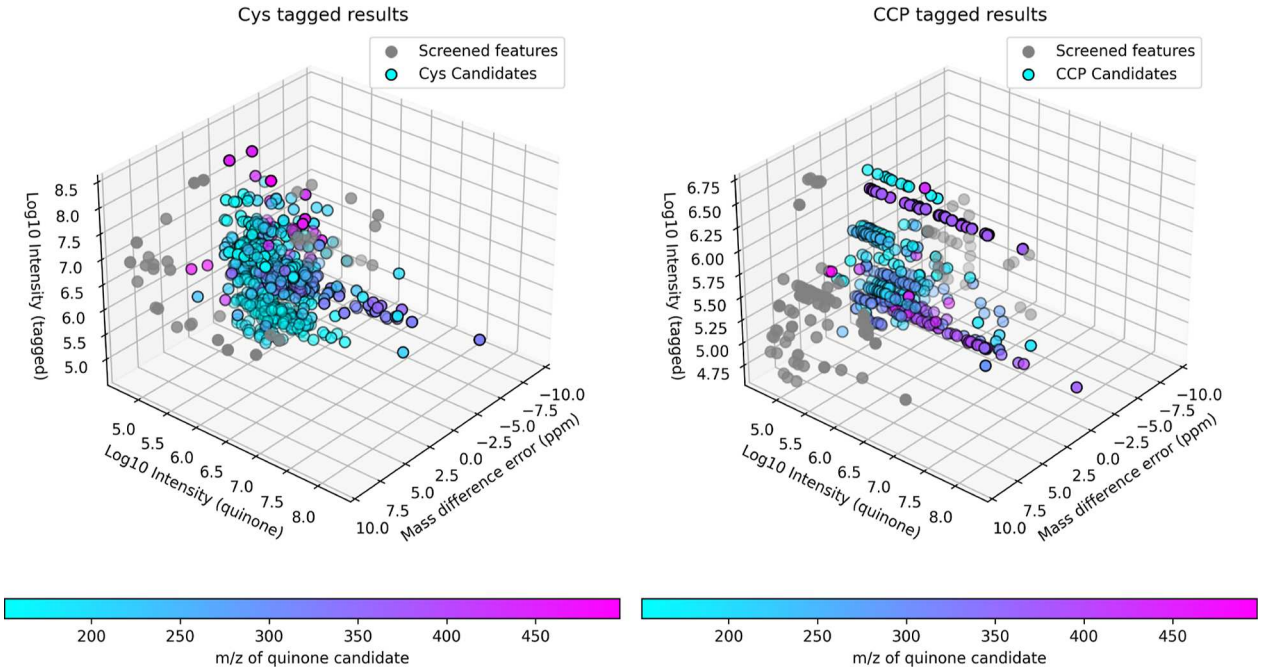

Figure 4. Mass difference ($\Delta m/z$) screening results, plotted mass difference error on the x-axis, log 10 quinone intensity on the y-axis, and log 10 Michael addition product intensity on the z-axis (m/z shown by colors) to identify pairs of apo quinone candidate and Michael addition production within 5 ppm error window: CCP tagged results shows pairs of quinone and Michael addition product with CCP and Cys tagged results shows pairs of quinone and Michael addition product with Cys.

Selectivity of Chemical Tagging. The tagging reaction was found to be selective to quinone functional groups for a 30 min reaction time at room temperature. The characteristic peaks of CnA, CaA, and CoA were captured at 274, 323, and 308 nm, respectively, which did not change after tagging with Cys, and no Michael addition products were observed for these compounds (Supporting Information, Table S4) (expected m/z of 267.057, 299.046, and 283.051, respectively, for potential products of CnA/CaA/CoA with Cys), indicating that Cys (includes thiol, carboxylic acid, and amino group) does not react substantially with carboxylic or phenolic functional groups in CnA/CaA/CoA (Figure S6). When 50 μM BQ was spiked in the mixtures of CnA/CaA/CoA, the MS peak for the BQ-Cys product was found, when the original UV peak for BQ at 245 nm disappeared, producing the UV peak for BQ-Cys at 301 nm, which was overridden by the mixture background. For lower concentrations (5 and 25 μM) of BQ spiked to the mixture, change in the original spectra was moderate to minimal (Figure 2). In TOF-MS analysis, the intensity of the BQ-Cys major peak (m/z = 230.048) was 7.4 $\times$ 10^5 $\pm$ 3.4 $\times$ 10^5 in the presence of 50 μM of co-occurring compounds versus 7.4 $\times$ 10^6 $\pm$ 2.3 $\times$ 10^6 in their absence, indicating suppression of BQ-Cys ionization in the complex matrix by one order. Such Michael addition reactions between the Michael acceptor and donor are lengthy processes, requiring 24 h or more to complete,[72] and often require base-catalyzed systems to facilitate the protonation, initiate, and continue the reactions.[73,74] Higher pH may favor this reaction by promoting deprotonation at unsaturated carbon. Quinones surrounded by two carbonyls in the same benzene rings are strong Michael acceptors that did not require catalysis and completed the reaction within 10−15 min under ambient conditions at neutral pH as we observed.[52,53]

Tagging Model Quinones in Water Extractions of Biochar. To validate the method for complex environmental samples, 10 μM BQ and NQ spiked in water extraction of biochars were tagged using Cys and CCP (Figure 3 and Table S5). The Michael addition products were successfully identified after tagging in complex matrices; however, the intensity of tagged products in complex matrices was 2−4 times lower than those in simple matrices (i.e., water). After the reaction with Cys and CCP in the SBE matrix, Cys-BQ, and Cys-NQ were detected at m/z of 230.0486 and 278.0479, with an average peak intensity of 406 $\pm$ 98 and 459 $\pm$ 165, respectively, compared to the intensity of 1656 $\pm$ 281 and 657 $\pm$ 302 for the products formed in the solution of only BQ or NQ. Similarly, CCP-BQ and CCP-NQ in the SBE matrix were captured at m/z of 1378.5247 and 1426.5187 with an average intensity of 5597 $\pm$ 645 and 5829 $\pm$ 1111, respectively, when the intensity of corresponding products formed in the solution of only BQ or NQ was 13,877 $\pm$ 1317 and 11,084 $\pm$ 353.

The efficiency of product formation can be affected by the selectivity and reactivity[75] of Cys and CCP among the various chemicals available in multicomponent systems or complex mixtures.[76] The steric effect of CCP with the thiol group might help to slow down the other reactions, providing more time to react with compounds, while Cys can be consumed substantially within a short period. As a result, the formation of Cys-quinone products and transformation due to further reaction in complex media can cause low Cys-quinone product intensity as we observed, though the Cys-quinone products (smaller molecules) are simpler than CCP-quinone products (larger molecules) for identification purpose. Also, tagging with CCP has the advantage that the background is cleaner for the range of m/z above 1000, while it might suffer from steric effects for relatively large quinones, which can be tagged more easily by Cys. To identify unknown quinones in complex environmental samples, tagging with Cys and CCP is found to be complementary to each other.

https://doi.org/10.1021/acs.est.4c04049
Environ. Sci. Technol. 2024, 58, 16432−16443

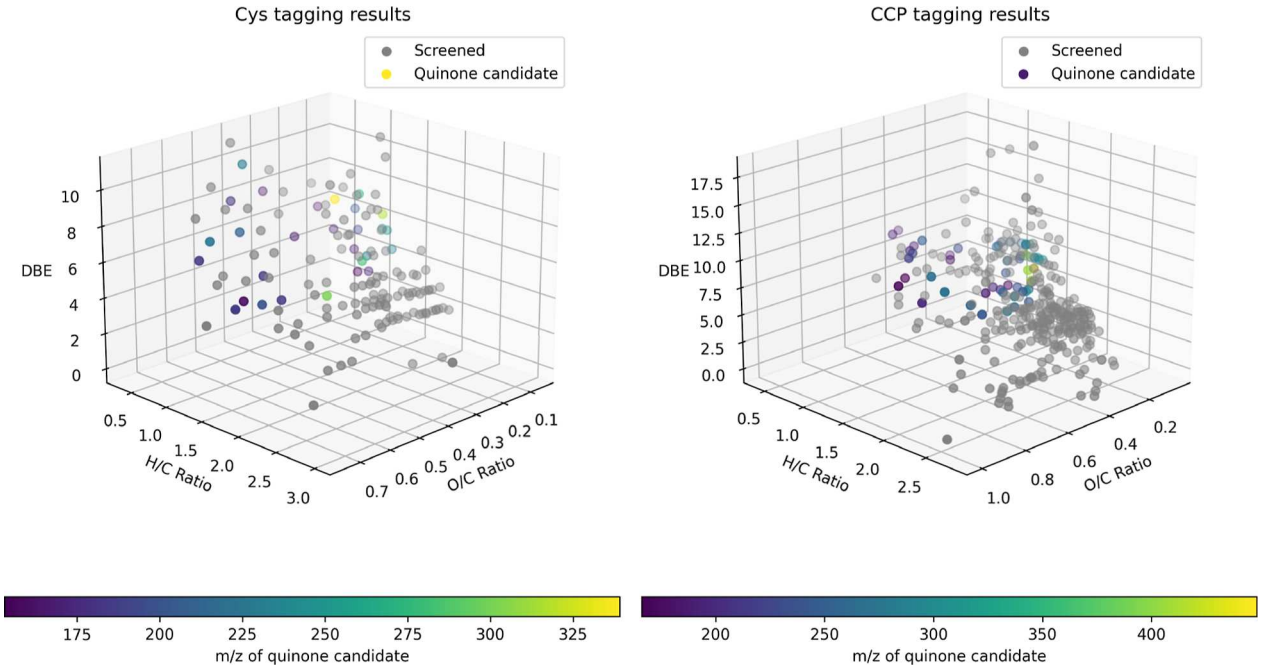

Figure 5. Van Krevelen diagram showing the quinone candidates: color intensity shows DBE of quinone candidates that meet screening criteria for quinones, i.e., DBE > 4, H/C < 1.9, and CoreMS confidence score > 0.59; candidates filtered/screened that do not meet the screening criteria for possible quinone shown in gray.

Quinones in SB Extracts. Mass difference ($\Delta m/z$) matching was used to capture the original peaks of the quinones ionizable with ESI ionization. These quinones were present in untagged CSBE and corresponded to distinct peaks following Michael addition. From 9780 features present in concentrated SB detected by ESI (+) ionization, molecular formulas were assigned accurately for 3481 features (Figure S7) using CoreMS. From total features, 4.08% (400) to 4.58% (448) of features were found to be tagged with CCP and Cys as captured by $\Delta m/z$ matching (Figure 4). From these, 400 and 448 pairs of possible quinone candidates and their possible Michael addition products were within the 5 ppm error window of $\Delta m/z$ matching, and pairs with greater than 5 ppm error were screened out.

Among the identified apo compounds and their Michael addition products, chemical formulas were predictable for 357 and 160 CCP-tagged and Cys-tagged candidates (Figure 5 and Table S6). After knowing the molecular formula for these candidates using CoreMS, minimum criteria were set to screen the quinone candidates: a minimum DBE value of 4 and a maximum H/C value of 1.9, based on the possible molecular composition of previously reported quinones (Figure S8).[77] In addition to that, candidates with low confidence scores (confidence score < 0.6 rejected) for chemical formula prediction were also screened out (Figure S9). From the screening of quinone candidates, 53 and 20 candidates were captured within a mass error of 5 ppm and tagged with CCP and Cys, respectively. The detected quinones had an average molecular size of 228.1031, ranging from 151.0753 with the molecular formula $C_9H_{10}O_2$ to 382.2949 with the molecular formula $C_{22}H_{39}O_4N_1$ (Tables S7 and S8). These candidate quinones had DBE ranging from 4 to 11, with an average of 5.6; their H/C ratio ranged from 0.4 to 1.86 and their O/C ratio from 0.09 to 0.56 (Figures 4 and S10), all falling within the range of quinones reported in the previous literature.[77] For the top eight high-intensity quinone candidates tagged with CCP and Cys, the unique Michael addition feature, the original apo quinone feature, and isotopic pattern validation for the calculated molecular formula are shown in Figure S11. No MS^2 was obtained for the identified candidates in this study for further validation and structure elucidation, which is our ongoing research and next-step priority.

■ ENVIRONMENTAL IMPLICATIONS

The analysis coupling chemical tagging with HRMS developed in this study can be used for identifying the chemical nature of quinones in natural and engineering systems, critical for the redox reactions, biogeochemical cycles of crucial elements [carbon (C), nitrogen (N), phosphorus (P), iron (Fe), and others], natural attenuation, and remediation of contaminated soils and waters. Quinones are very important components of pyrogenic carbons in soils, especially those impacted by wildfires, and can play an important role in regulating the biogeochemical processes and functions of watersheds.

Quinones can be important not only for the biogeochemistry of critical elements but also for water quality evaluation. Recent studies have uncovered that chlorinated or brominated quinones are among the most toxic disinfection byproducts,[78] for which quinones can be the most critical precursors. Emerging quinone-based toxicants, such as 6PPD-quinones, with large-scale impacts, were also discovered.[79] However, quinones in natural soil and water environments are still mainly a black box. The method developed in this study can be of great value to uncover their chemical structures and properties. HRMS analysis applied in this study has already identified a list of candidates for quinones in biochar extracts, which is subject to further investigation and validation. While no MS/MS was obtained for the identified candidates of quinones in biochar extractions in this study, the analysis determined 20 (based on tagging with Cys) and 53 (based on tagging with CCP) possible candidates of quinones for the next step analysis and validation. Potential further identification and

https://doi.org/10.1021/acs.est.4c04049
Environ. Sci. Technol. 2024, 58, 16432−16443

validation of quinones in natural environmental media, such as biochars or similar pyrogenic carbons generated from wildfires, can provide insights into their roles in important environmental biogeochemical reactions and help more accurately simulate the reactive transport of critical elements, especially under the impact of wildfires and climate change. Determination of possible quinone candidates can also provide important information for understanding and protecting water quality from the influences of wildfire. Such information about the critical components of biochars can enable optimized applications.

Due to intentional biochar application[80] or char formation during wildfires,[81] water extractable pyrogenic carbon has significant contribution to NOM. While NOM contains molecules with higher aliphatic properties than pyrogenic carbon, they share a common range of H/C and O/C values with water extractions of biochar as reported by previous studies, e.g., with H/C (∼0.4−2.2) and O/C (∼0.1−0.9) for biochar, and H/C (∼0.4−2.2) and O/C (∼0−1) for NOM.[82,83] So, this method can be potentially expanded to other complex environmental (NOM) samples mixed with pyrogenic carbon as a source for quinones. Further investigations are needed to optimize the application of the developed method for quinones in a more diverse NOM.

■ ASSOCIATED CONTENT

Supporting Information

The Supporting Information is available free of charge at https://pubs.acs.org/doi/10.1021/acs.est.4c04049.

Michael addition reaction, reaction kinetics, method schematic, isotope pattern of model quinones, UV and MS spectra of nonquinones, accuracy of molecular formula prediction using CoreMS, van Krevelen diagram of the previously reported and identified quinones, molecular distribution of quinone candidates, spectra of top eight candidates, experimental setup, model quinone's quantitative data, and the list of identified quinone candidates (PDF)

■ AUTHOR INFORMATION

Corresponding Author

Yu Yang − *Department of Civil and Environmental Engineering, University of Nevada, Reno, Reno, Nevada 89523, United States;* orcid.org/0000-0002-7568-0202; Email: yuy@unr.edu

Authors

Anil Timilsina − *Department of Civil and Environmental Engineering, University of Nevada, Reno, Reno, Nevada 89523, United States;* orcid.org/0000-0001-7053-0662

Srinidhi Lokesh − *Department of Civil and Environmental Engineering, University of Nevada, Reno, Reno, Nevada 89523, United States*

Abrar Shahriar − *Department of Civil and Environmental Engineering, University of Nevada, Reno, Reno, Nevada 89523, United States*

Travis Numan − *Department of Civil and Environmental Engineering, University of Nevada, Reno, Reno, Nevada 89523, United States*

Tilman Schramm − *CMFI Cluster of Excellence, University of Tuebingen, 72076 Tuebingen, Germany; Department of Biochemistry, University of California Riverside, Riverside, California 92507, United States*

Paolo Stincone − *CMFI Cluster of Excellence, University of Tuebingen, 72076 Tuebingen, Germany;* orcid.org/0000-0002-2214-6655

Laurinda Korang Nyarko − *School of Chemical, Biological, and Environmental Engineering, Oregon State University, Corvallis, Oregon 97331, United States*

Christian Dewey − *Department of Chemistry, University of Minnesota, Minneapolis, Minnesota 55455, United States*

Rene Boiteau − *Department of Chemistry, University of Minnesota, Minneapolis, Minnesota 55455, United States;* orcid.org/0000-0002-4127-4417

Daniel Petras − *CMFI Cluster of Excellence, University of Tuebingen, 72076 Tuebingen, Germany; Department of Biochemistry, University of California Riverside, Riverside, California 92507, United States*

Complete contact information is available at: https://pubs.acs.org/10.1021/acs.est.4c04049

Notes

The authors declare no competing financial interest.

■ ACKNOWLEDGMENTS

This study was supported by funding from the National Science Foundation Awards (NSF nos. 2108270 and 1804209). We also acknowledge Dr. Ruprecht and Dr. Spain at the Shared Facility in the Department of Chemistry at the University of Nevada, Reno for help with TOF-MS. P.S. was supported by the European Union's Horizon Europe research and innovation program through a Marie Skłodowska-Curie fellowship (n.101108450-MeStaLeM).

■ REFERENCES

(1) Xu, W.; Walpen, N.; Keiluweit, M.; Kleber, M.; Sander, M. Redox Properties of Pyrogenic Dissolved Organic Matter (pyDOM) from Biomass-Derived Chars. *Environ. Sci. Technol.* **2021**, *55* (16), 11434−11444.

(2) Walpen, N.; Getzinger, G. J.; Schroth, M. H.; Sander, M. Electron-Donating Phenolic and Electron-Accepting Quinone Moieties in Peat Dissolved Organic Matter: Quantities and Redox Transformations in the Context of Peat Biogeochemistry. *Environ. Sci. Technol.* **2018**, *52* (9), 5236−5245.

(3) Sun, T.; Levin, B. D. A.; Schmidt, M. P.; Guzman, J. J. L.; Enders, A.; Martinez, C. E.; Muller, D. A.; Angenent, L. T.; Lehmann, J. Simultaneous Quantification of Electron Transfer by Carbon Matrices and Functional Groups in Pyrogenic Carbon. *Environ. Sci. Technol.* **2018**, *52* (15), 8538−8547.

(4) Sun, T.; Levin, B. D.; Guzman, J. J.; Enders, A.; Muller, D. A.; Angenent, L. T.; Lehmann, J. Rapid electron transfer by the carbon matrix in natural pyrogenic carbon. *Nat. Commun.* **2017**, *8* (1), 14873.

(5) Lovley, D. R.; Coates, J. D.; Blunt-Harris, E. L.; Phillips, E. J.; Woodward, J. C. Humic substances as electron acceptors for microbial respiration. *Nature* **1996**, *382* (6590), 445−448.

(6) Aeschbacher, M.; Vergari, D.; Schwarzenbach, R. P.; Sander, M. Electrochemical analysis of proton and electron transfer equilibria of the reducible moieties in humic acids. *Environ. Sci. Technol.* **2011**, *45* (19), 8385−8394.

(7) Lovley, D. R.; Blunt-Harris, E. L. Role of humic-bound iron as an electron transfer agent in dissimilatory Fe (III) reduction. *Appl. Environ. Microbiol.* **1999**, *65* (9), 4252−4254.

(8) Wolf, M.; Kappler, A.; Jiang, J.; Meckenstock, R. U. Effects of humic substances and quinones at low concentrations on ferrihydrite reduction by Geobacter metallireducens. *Environ. Sci. Technol.* **2009**, *43* (15), 5679−5685.

(9) Scott, D. T.; McKnight, D. M.; Blunt-Harris, E. L.; Kolesar, S. E.; Lovley, D. R. Quinone moieties act as electron acceptors in the reduction of humic substances by humics-reducing microorganisms. *Environ. Sci. Technol.* **1998**, *32* (19), 2984−2989.
(10) O'Loughlin, E. J. Effects of electron transfer mediators on the bioreduction of lepidocrocite (gamma-FeOOH) by Shewanella putrefaciens CN32. *Environ. Sci. Technol.* **2008**, *42* (18), 6876−6882.
(11) Bond, D. R.; Lovley, D. R. Reduction of Fe(III) oxide by methanogens in the presence and absence of extracellular quinones. *Environ. Microbiol.* **2002**, *4* (2), 115−124.
(12) Blodau, C. Carbon cycling in peatlands A review of processes and controls. *Environ. Rev.* **2002**, *10* (2), 111−134.
(13) Stein, L. Y.; Klotz, M. G. The nitrogen cycle. *Curr. Biol.* **2016**, *26* (3), R94−R98.
(14) Peretyazhko, T.; Sposito, G. Iron (III) reduction and phosphorous solubilization in humid tropical forest soils. *Geochim. Cosmochim. Acta* **2005**, *69* (14), 3643−3652.
(15) Li, Y.; Yu, S.; Strong, J.; Wang, H. Are the biogeochemical cycles of carbon, nitrogen, sulfur, and phosphorus driven by the "FeIII−FeII redox wheel" in dynamic redox environments? *J. Soils Sediments* **2012**, *12* (5), 683−693.
(16) Gupta, V.; Smemo, K. A.; Yavitt, J. B.; Fowle, D.; Branfireun, B.; Basiliko, N. Stable isotopes reveal widespread anaerobic methane oxidation across latitude and peatland type. *Environ. Sci. Technol.* **2013**, *47* (15), 8273−8279.
(17) Smemo, K.; Yavitt, J. Anaerobic oxidation of methane: an underappreciated aspect of methane cycling in peatland ecosystems? *Biogeosciences* **2011**, *8* (3), 779−793.
(18) Scheller, S.; Yu, H.; Chadwick, G. L.; McGlynn, S. E.; Orphan, V. J. Artificial electron acceptors decouple archaeal methane oxidation from sulfate reduction. *Science* **2016**, *351* (6274), 703−707.
(19) Valenzuela, E. I.; Prieto-Davo, A.; Lopez-Lozano, N. E.; Hernandez-Eligio, A.; Vega-Alvarado, L.; Juarez, K.; Garcia-Gonzalez, A. S.; Lopez, M. G.; Cervantes, F. J. Anaerobic Methane Oxidation Driven by Microbial Reduction of Natural Organic Matter in a Tropical Wetland. *Appl. Environ. Microbiol.* **2017**, *83* (11), No. e00645-17.
(20) Blodau, C.; Deppe, M. Humic acid addition lowers methane release in peats of the Mer Bleue bog, Canada. *Soil Biol. Biochem.* **2012**, *52*, 96−98.
(21) Keller, J. K.; Weisenhorn, P. B.; Megonigal, J. P. Humic acids as electron acceptors in wetland decomposition. *Soil Biol. Biochem.* **2009**, *41* (7), 1518−1522.
(22) Roden, E. E.; Kappler, A.; Bauer, I.; Jiang, J.; Paul, A.; Stoesser, R.; Konishi, H.; Xu, H. Extracellular electron transfer through microbial reduction of solid-phase humic substances. *Nat. Geosci.* **2010**, *3* (6), 417−421.
(23) Newman, D. K.; Kolter, R. A role for excreted quinones in extracellular electron transfer. *Nature* **2000**, *405* (6782), 94−97.
(24) Jiang, C.; Garg, S.; Waite, T. D. Hydroquinone-mediated redox cycling of iron and concomitant oxidation of hydroquinone in oxic waters under acidic conditions: Comparison with iron−natural organic matter interactions. *Environ. Sci. Technol.* **2015**, *49* (24), 14076−14084.
(25) Wendlandt, A. E.; Stahl, S. S. Quinone-Catalyzed Selective Oxidation of Organic Molecules. *Angew. Chem., Int. Ed. Engl.* **2015**, *54* (49), 14638−14658.
(26) Leon, M. A.; Liu, X.; Phan, J. H.; Clift, M. D. Amine Functionalization through Sequential Quinone-Catalyzed Oxidation/Nucleophilic Addition. *Eur. J. Org Chem.* **2016**, *2016* (26), 4508−4515.
(27) Zhang, R.; Luo, S. Bio-inspired quinone catalysis. *Chin. Chem. Lett.* **2018**, *29* (8), 1193−1200.
(28) Doong, R. A.; Chiang, H. C. Transformation of carbon tetrachloride by thiol reductants in the presence of quinone compounds. *Environ. Sci. Technol.* **2005**, *39* (19), 7460−7468.
(29) Curtis, G. P.; Reinhard, M. Reductive dehalogenation of hexachloroethane, carbon tetrachloride, and bromoform by anthrahydroquinone disulfonate and humic Acid. *Environ. Sci. Technol.* **1994**, *28* (13), 2393−2401.
(30) Perlinger, J. A.; Angst, W.; Schwarzenbach, R. P. Kinetics of the reduction of hexachloroethane by juglone in solutions containing hydrogen sulfide. *Environ. Sci. Technol.* **1996**, *30* (12), 3408−3417.
(31) Wang, C.-J.; Thiele, S.; Bollag, J.-M. Interaction of 2,4,6-trinitrotoluene (TNT) and 4-amino-2,6-dinitrotoluene with humic monomers in the presence of oxidative enzymes. *Arch. Environ. Contam. Toxicol.* **2002**, *42* (1), 1−8.
(32) Thorn, K. A.; Kennedy, K. R. 15N NMR investigation of the covalent binding of reduced TNT amines to soil humic acid, model compounds, and lignocellulose. *Environ. Sci. Technol.* **2002**, *36* (17), 3787−3796.
(33) Fang, G.; Gao, J.; Dionysiou, D. D.; Liu, C.; Zhou, D. Activation of persulfate by quinones: free radical reactions and implication for the degradation of PCBs. *Environ. Sci. Technol.* **2013**, *47* (9), 4605−4611.
(34) Zhou, Y.; Jiang, J.; Gao, Y.; Ma, J.; Pang, S. Y.; Li, J.; Lu, X. T.; Yuan, L. P. Activation of Peroxymonosulfate by Benzoquinone: A Novel Nonradical Oxidation Process. *Environ. Sci. Technol.* **2015**, *49* (21), 12941−12950.
(35) Ortiz-Bernad, I.; Anderson, R. T.; Vrionis, H. A.; Lovley, D. R. Vanadium respiration by Geobacter metallireducens: novel strategy for in situ removal of vanadium from groundwater. *Appl. Environ. Microbiol.* **2004**, *70* (5), 3091−3095.
(36) Kwon, M. J.; Finneran, K. T. Biotransformation products and mineralization potential for hexahydro-1,3,5-trinitro-1,3,5-triazine (RDX) in abiotic versus biological degradation pathways with anthraquinone-2,6-disulfonate (AQDS) and Geobacter metallireducens. *Biodegradation* **2008**, *19* (5), 705−715.
(37) Xu, H.; Xiao, L.; Zheng, S.; Zhang, Y.; Li, J.; Liu, F. Reductive degradation of chloramphenicol by Geobacter metallireducens. *Sci. China: Technol. Sci.* **2019**, *62* (10), 1688−1694.
(38) Voordeckers, J. W.; Kim, B. C.; Izallalen, M.; Lovley, D. R. Role of Geobacter sulfurreducens outer surface c-type cytochromes in reduction of soil humic acid and anthraquinone-2,6-disulfonate. *Appl. Environ. Microbiol.* **2010**, *76* (7), 2371−2375.
(39) Lovley, D. R.; Fraga, J. L.; Coates, J. D.; Blunt-Harris, E. L. Humics as an electron donor for anaerobic respiration. *Environ. Microbiol.* **1999**, *1* (1), 89−98.
(40) Lokesh, S.; Kim, J.; Zhou, Y.; Wu, D.; Pan, B.; Wang, X.; Behrens, S.; Huang, C.-H.; Yang, Y. Anaerobic dehalogenation by reduced aqueous biochars. *Environ. Sci. Technol.* **2020**, *54* (23), 15142−15150.
(41) Lokesh, S.; Lard, M. L.; Cook, R. L.; Yang, Y. Critical Role of Semiquinones in Reductive Dehalogenation. *Environ. Sci. Technol.* **2023**, *57* (38), 14218−14225.
(42) Royer, R. A.; Burgos, W. D.; Fisher, A. S.; Unz, R. F.; Dempsey, B. A. Enhancement of biological reduction of hematite by electron shuttling and Fe(II) complexation. *Environ. Sci. Technol.* **2002**, *36* (9), 1939−1946.
(43) Li, X.; Guo, W.; Liu, Z.; Wang, R.; Liu, H. Quinone-modified NH2-MIL-101 (Fe) composite as a redox mediator for improved degradation of bisphenol A. *J. Hazard. Mater.* **2017**, *324*, 665−672.
(44) Xu, J.; Zhuang, L.; Yang, G.; Yuan, Y.; Zhou, S. Extracellular quinones affecting methane production and methanogenic community in paddy soil. *Microb. Ecol.* **2013**, *66* (4), 950−960.
(45) Zweier, J. L.; Flaherty, J. T.; Weisfeldt, M. L. Direct measurement of free radical generation following reperfusion of ischemic myocardium. *Proc. Natl. Acad. Sci. U.S.A.* **1987**, *84* (5), 1404−1407.
(46) Dyall, L.; Winstein, S. Nuclear magnetic resonance spectra and characterization of some quinone methides. *J. Am. Chem. Soc.* **1972**, *94* (7), 2196−2199.
(47) Simon, C.; Duhrkop, K.; Petras, D.; Roth, V. N.; Bocker, S.; Dorrestein, P. C.; Gleixner, G. Mass Difference Matching Unfolds Hidden Molecular Structures of Dissolved Organic Matter. *Environ. Sci. Technol.* **2022**, *56* (15), 11027−11040.

(48) Lambidis, S. P.; Schramm, T.; Steuer-Lodd, K.; Farrell, S.; Stincone, P.; Schmid, R.; Koester, I.; Torres, R.; Aluwihare, L.; Simon, C.; Petras, D. Two-Dimensional Liquid Chromatography Tandem-Mass Spectrometry Untangles the Deep Metabolome of Marine Dissolved Organic Matter. *ChemRxiv* **2023**.
(49) Leenheer, J. A.; Croué, J. P. Peer reviewed: characterizing aquatic dissolved organic matter. *Environ. Sci. Technol.* **2003**, *37* (1), 18A−26A.
(50) Zark, M.; Dittmar, T. Universal molecular structures in natural dissolved organic matter. *Nat. Commun.* **2018**, *9* (1), 3178.
(51) Minor, E. C.; Swenson, M. M.; Mattson, B. M.; Oyler, A. R. Structural characterization of dissolved organic matter: a review of current techniques for isolation and analysis. *Environ. Sci.: Processes Impacts* **2014**, *16* (9), 2064−2079.
(52) Ma, R.; Hu, J.; Cai, Z.; Ju, H. Dual quinone tagging for MALDI-TOF mass spectrometric quantitation of cysteine-containing peptide. *Anal. Chem.* **2014**, *86* (16), 8275−8280.
(53) Timilsina, A.; Lokesh, S.; Shahriar, A.; Numan, T.; Yang, Y. Quantification of Quinones in Environmental Media by Chemical Tagging with Cysteine-Containing Peptides Coupled to Size Exclusionary Separation. *Anal. Chem.* **2023**, *95* (34), 12575−12579.
(54) Stincone, P.; Pakkir Shah, A. K.; Schmid, R.; Graves, L. G.; Lambidis, S. P.; Torres, R. R.; Xia, S. N.; Minda, V.; Aron, A. T.; Wang, M.; Hughes, C. C.; Petras, D. Evaluation of Data-Dependent MS/MS Acquisition Parameters for Non-Targeted Metabolomics and Molecular Networking of Environmental Samples: Focus on the Q Exactive Platform. *Anal. Chem.* **2023**, *95* (34), 12673−12682.
(55) Schmid, R.; Heuckeroth, S.; Korf, A.; Smirnov, A.; Myers, O.; Dyrlund, T. S.; Bushuiev, R.; Murray, K. J.; Hoffmann, N.; Lu, M.; Sarvepalli, A.; Zhang, Z.; Fleischauer, M.; Duhrkop, K.; Wesner, M.; Hoogstra, S. J.; Rudt, E.; Mokshyna, O.; Brungs, C.; Ponomarov, K.; Mutabdzija, L.; Damiani, T.; Pudney, C. J.; Earll, M.; Helmer, P. O.; Fallon, T. R.; Schulze, T.; Rivas-Ubach, A.; Bilbao, A.; Richter, H.; Nothias, L. F.; Wang, M.; Oresic, M.; Weng, J. K.; Bocker, S.; Jeibmann, A.; Hayen, H.; Karst, U.; Dorrestein, P. C.; Petras, D.; Du, X.; Pluskal, T. Integrative analysis of multimodal mass spectrometry data in MZmine 3. *Nat. Biotechnol.* **2023**, *41* (4), 447−449.
(56) Myers, O. D.; Sumner, S. J.; Li, S.; Barnes, S.; Du, X. One Step Forward for Reducing False Positive and False Negative Compound Identifications from Mass Spectrometry Metabolomics Data: New Algorithms for Constructing Extracted Ion Chromatograms and Detecting Chromatographic Peaks. *Anal. Chem.* **2017**, *89* (17), 8696−8703.
(57) Dührkop, K.; Nothias, L.-F.; Fleischauer, M.; Reher, R.; Ludwig, M.; Hoffmann, M. A.; Petras, D.; Gerwick, W. H.; Rousu, J.; Dorrestein, P. C.; et al. Systematic classification of unknown metabolites using high-resolution fragmentation mass spectra. *Nat. Biotechnol.* **2021**, *39* (4), 462−471.
(58) NIST Hydroquinone. NIST Chemistry WebBook, SRD 69. https://webbook.nist.gov/cgi/cbook.cgi?ID=C123319&Mask=400#UV-Vis-Spec (accessed May 12).
(59) Jongberg, S.; Gislason, N. E.; Lund, M. N.; Skibsted, L. H.; Waterhouse, A. L. Thiol−quinone adduct formation in myofibrillar proteins detected by LC-MS. *J. Agric. Food Chem.* **2011**, *59* (13), 6900−6905.
(60) Zhang, P.; Chan, W.; Ang, I. L.; Wei, R.; Lam, M. M. T.; Lei, K. M. K.; Poon, T. C. W. Revisiting Fragmentation Reactions of Protonated α-Amino Acids by High-Resolution Electrospray Ionization Tandem Mass Spectrometry with Collision-Induced Dissociation. *Sci. Rep.* **2019**, *9* (1), 6453.
(61) Domingo, L. R. Molecular Electron Density Theory: A Modern View of Reactivity in Organic Chemistry. *Molecules* **2016**, *21* (10), 1319.
(62) Domingo, L. R.; Rios-Gutierrez, M. A Molecular Electron Density Theory Study of the Reactivity of Azomethine Imine in [3 + 2] Cycloaddition Reactions. *Molecules* **2017**, *22* (5), 750.
(63) Chen, X.; Dong, Y.; Yu, X.; Wang, Z.; Liu, Y.; Liu, J.; Yao, S. Steric hindrance of methyl group on the reaction pathway of hydrodesulfurization in the presence of quinoline. *Catal. Lett.* **2021**, *151* (1), 194−211.
(64) Chatfield, D. C.; Augsten, A.; D'Cunha, C.; Lewandowska, E.; Wnuk, S. F. Theoretical and experimental study of the regioselectivity of Michael additions. *Eur. J. Org Chem.* **2004**, *2004* (2), 313−322.
(65) Miladinovic, S. M.; Fornelli, L.; Lu, Y.; Piech, K. M.; Girault, H. H.; Tsybin, Y. O. In-spray supercharging of peptides and proteins in electrospray ionization mass spectrometry. *Anal. Chem.* **2012**, *84* (11), 4647−4651.
(66) Lifshitz, C.; Laskin, J. *Principles of Mass Spectrometry Applied to Biomolecules*; John Wiley & Sons, 2006.
(67) El-Najjar, N.; Gali-Muhtasib, H.; Ketola, R. A.; Vuorela, P.; Urtti, A.; Vuorela, H. The chemical and biological activities of quinones: overview and implications in analytical detection. *Phytochem. Rev.* **2011**, *10*, 353−370.
(68) Zhang, H.; Chobot, S. E.; Osyczka, A.; Wraight, C. A.; Dutton, P. L.; Moser, C. C. Quinone and non-quinone redox couples in Complex III. *J. Bioenerg. Biomembr.* **2008**, *40* (5), 493−499.
(69) Devlin, H. R.; Harris, I. J. Mechanism of the oxidation of aqueous phenol with dissolved oxygen. *Ind. Eng. Chem. Fundam.* **1984**, *23* (4), 387−392.
(70) Ishikita, H.; Knapp, E.-W. Redox potential of quinones in both electron transfer branches of photosystem I. *J. Biol. Chem.* **2003**, *278* (52), 52002−52011.
(71) Roginsky, V.; Barsukova, T. Kinetics of oxidation of hydroquinones by molecular oxygen. Effect of superoxide dismutase. *J. Chem. Soc., Perkin Trans. 2* **2000**, *2* (7), 1575−1582.
(72) Hoffmann, M.; Mikutta, C.; Kretzschmar, R. Bisulfide reaction with natural organic matter enhances arsenite sorption: insights from X-ray absorption spectroscopy. *Environ. Sci. Technol.* **2012**, *46* (21), 11788−11797.
(73) Nair, D. P.; Podgorski, M.; Chatani, S.; Gong, T.; Xi, W.; Fenoli, C. R.; Bowman, C. N. The thiol-Michael addition click reaction: a powerful and widely used tool in materials chemistry. *Chem. Mater.* **2014**, *26* (1), 724−744.
(74) Chan, J. W.; Hoyle, C. E.; Lowe, A. B.; Bowman, M. Nucleophile-initiated thiol-Michael reactions: effect of organocatalyst, thiol, and ene. *Macromolecules* **2010**, *43* (15), 6381−6388.
(75) Chatani, S.; Nair, D. P.; Bowman, C. N. Relative reactivity and selectivity of vinyl sulfones and acrylates towards the thiol−Michael addition reaction and polymerization. *Polym. Chem.* **2013**, *4* (4), 1048−1055.
(76) Huang, S.; Sinha, J.; Podgórski, M.; Zhang, X.; Claudino, M.; Bowman, C. N. Mechanistic Modeling of the Thiol−Michael Addition Polymerization Kinetics: Structural Effects of the Thiol and Vinyl Monomers. *Macromolecules* **2018**, *51* (15), 5979−5988.
(77) Song, Y.; Buettner, G. R. Thermodynamic and kinetic considerations for the reaction of semiquinone radicals to form superoxide and hydrogen peroxide. *Free Radicals Biol. Med.* **2010**, *49* (6), 919−962.
(78) Zhao, Y.; Anichina, J.; Lu, X.; Bull, R. J.; Krasner, S. W.; Hrudey, S. E.; Li, X. F. Occurrence and formation of chloro- and bromo-benzoquinones during drinking water disinfection. *Water Res.* **2012**, *46* (14), 4351−4360.
(79) Tian, Z.; Zhao, H.; Peter, K. T.; Gonzalez, M.; Wetzel, J.; Wu, C.; Hu, X.; Prat, J.; Mudrock, E.; Hettinger, R.; et al. A ubiquitous tire rubber−derived chemical induces acute mortality in coho salmon. *Science* **2021**, *371* (6525), 185−189.
(80) Sakhiya, A. K.; Anand, A.; Kaushal, P. Production, activation, and applications of biochar in recent times. *Biochar* **2020**, *2*, 253−285.
(81) Agbeshie, A. A.; Abugre, S.; Atta-Darkwa, T.; Awuah, R. A review of the effects of forest fire on soil properties. *J. For. Res.* **2022**, *33* (5), 1419−1441.
(82) McKenna, A. M.; Chacon-Patino, M. L.; Chen, H.; Blakney, G. T.; Mentink-Vigier, F.; Young, R. B.; Ippolito, J. A.; Borch, T. Expanding the Analytical Window for Biochar Speciation: Molecular Comparison of Solvent Extraction and Water-Soluble Fractions of Biochar by FT-ICR Mass Spectrometry. *Anal. Chem.* **2021**, *93* (46), 15365−15372.

(83) Bahureksa, W.; Tfaily, M. M.; Boiteau, R. M.; Young, R. B.; Logan, M. N.; McKenna, A. M.; Borch, T. Soil Organic Matter Characterization by Fourier Transform Ion Cyclotron Resonance Mass Spectrometry (FTICR MS): A Critical Review of Sample Preparation, Analysis, and Data Interpretation. *Environ. Sci. Technol.* **2021**, *55* (14), 9637−9656.

https://doi.org/10.1021/acs.est.4c04049
Environ. Sci. Technol. 2024, 58, 16432−16443